ACS APPLIED NANO MATERIALS
Cite This: ACS Appl. Nano Mater. 2019, 2, 1146−1151
Letter
www.acsanm.org

Hierarchically Structured Nanoparticle Monolayers for the Tailored Etching of Nanoporous Silicon

Methely Sharma,[†,§] Alvin T.L. Tan,[†,§] Brendan D. Smith,[†] A. John Hart,[*,‡] and Jeffrey C. Grossman[*,†]

[†]Department of Materials Science and Engineering and [‡]Department of Mechanical Engineering, Massachusetts Institute of Technology, Cambridge, Massachusetts 02139, United States

Supporting Information

ABSTRACT: Nanoporous silicon (NPSi) can be used in a wide range of applications including nanofiltration, thermoelectrics, photovoltaics, and catalysis. Metal-assisted chemical etching (MACE) is an electrochemical, solution-based NPSi fabrication process that relies on control over catalyst deposition to obtain the desired porous structure. In this paper, blade-casting is explored as a template-free, self-assembly deposition technique for MACE catalyst. Mixtures of silica (SiO_2) and gold-core silica-shell nanoparticle (SiO_2AuNP) catalysts are assembled by blade-casting, resulting in tunable hierarchical monolayers that, after MACE, produce >100 μm^2 NPSi with ∼20 nm pores.

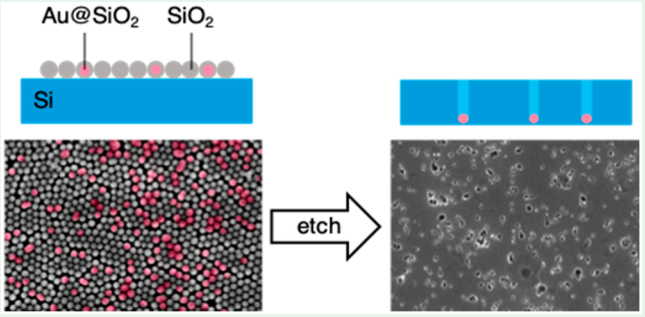

KEYWORDS: *self-assembly, nanoporous silicon, metal-assisted chemical etching, blade-casting, nanofabrication*

Recently, nanoporous silicon (NPSi) has emerged as a promising material for a variety of applications including photovoltaics,[1,2] nanofiltration,[3−5] thermoelectrics,[6,7] and catalysis.[8] While there are numerous lithographic and maskless chemical etching methods available for the production of NPSi, an approach known as metal-assisted chemical etching (MACE) has recently received significant attention for its ability to produce porous silicon with controllable pore size and spacing in a wet-etch-based manner, allowing for scalable processing.[9] The MACE process involves two steps. In brief, a noble-metal catalyst is first deposited on the surface of Si (e.g., a wafer), after which the material is immersed in an aqueous solution of hydrogen peroxide (H_2O_2) and hydrofluoric acid (HF). H_2O_2 is reduced at the noble metal surface, injecting a hole that diffuses to the metal−Si interface and oxidizes Si locally within close proximity of the catalyst. The immediate dissolution of this oxide by HF and the further consumption of the underlying Si in this manner results in the production of negative features closely mirroring the shape of the initial metal catalyst. Directional etching is achievable through the selection of Si lattice orientation, where etch anisotropy occurs preferentially in the <100> and <110> directions due to the breaking of a minimal number of Si back bonds relative to the <111> directions.

While a number of studies have investigated the use of noble metal nanoparticles as effective MACE catalysts in the production of NPSi, it has been challenging to deposit homogeneously spaced nanometer-scale particles over macroscale areas while avoiding aggregation. Our previous work introduced such an approach via the drop-casting of aqueous suspensions of gold-core silica-shell nanoparticle (SiO_2AuNP) catalysts,[8] demonstrating the ability to maintain catalyst spacing with sacrificial silica shells over tens of square microns.

A challenge in nanofabrication, not only in the MACE process but also in general, is the controlled positioning of diverse nanoparticles to create functional structures. Often, as is the case for NPSi production, a monolayer of nanoparticles is a desirable structure and is obtainable through methods such as drop-casting,[10,11] spin-coating,[12,13] and Langmuir−Blodgett assembly.[14,15] Numerous studies have elucidated a major limitation of drop-casting as a method for forming large-area monolayers reproducibly. Typically, when the droplet evaporates, the meniscus of the droplet is pinned at the contact line,[10] where the rate of evaporation is the highest. Therefore, a "coffee ring" of dense multilayers is deposited at the periphery of the droplet and sparse regions of particle islands are formed at the center of the droplet, as illustrated in Figure 1a and shown in Figure S1. In our previous work, SiO_2AuNP catalyst particles were drop-cast to illustrate the potential of utilizing silica shells as effective spacers for <20 nm pore NPSi fabrication.[8] However, for such a technique to be useful in applications, a much-more-uniform, large-area, and controllable approach is needed for the catalyst deposition prior to the etching process. In particular, we believe that a technique for achieving tunable pore density in areas exceeding 100 μm^2 on a silicon platform is nontrivial and of practical importance.

Received: February 4, 2019
Accepted: February 20, 2019
Published: February 20, 2019

DOI: 10.1021/acsanm.9b00184
ACS Appl. Nano Mater. 2019, 2, 1146−1151

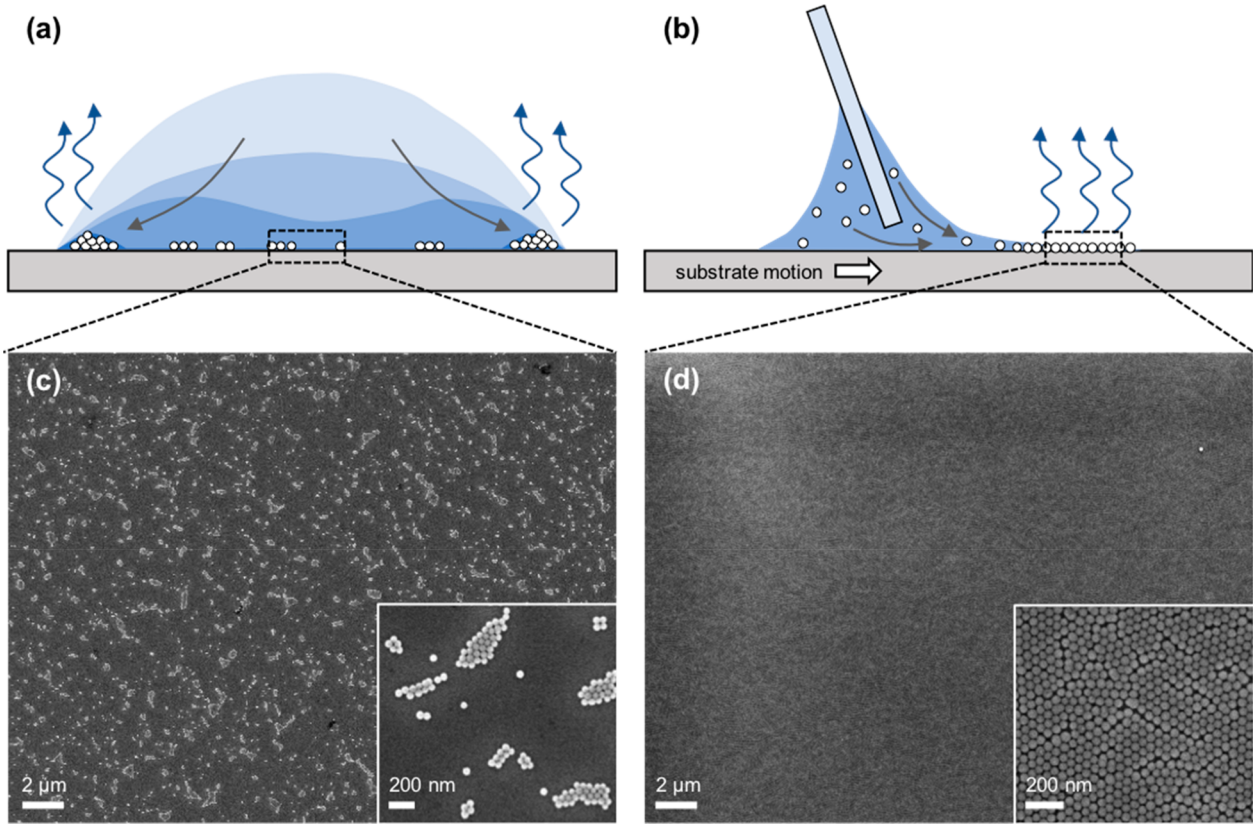

Figure 1. Evaporative self-assembly by drop-casting and blade-casting. (a) Illustration of drop-casting in which evaporation is highest at the edge of the droplet, resulting in thick "coffee-ring" deposits at the edge and sparse particle islands at the middle of the drop. (b) Illustration of blade-casting in which a blade is used to draw the meniscus laterally across the substrate, resulting in uniform evaporative self-assembly of particles at the trailing edge. (c, d) SEM of particle deposits formed by (c) drop-casting and (d) blade-casting.

In this paper, we utilize blade-casting as an alternative approach to the deposition of large-area SiO_2AuNP monolayers for MACE of Si. In blade-casting, a blade is used to draw the meniscus laterally across the substrate so as to maintain uniform self-assembly of the colloidal particles,[16] as illustrated in Figure 1b. Blade-casting is an attractive means for scaling up because it is a well-established process that can be designed to be continuous and, in principle, is capable of coating an indefinite length of substrate with 100% of the particles ending up in the final assembly.

We deposited aqueous solutions of 10 nm SiO_2AuNP (6.7×10^{12} particles per milliliter) onto silicon substrates by drop-casting and blade-casting. Exemplary results are shown in Figure 1. Indeed, the drop-cast SiO_2AuNPs assembled into a coffee-ring pattern, with thick deposits at the edge and sparse deposits in the middle of the droplet. Scanning electron microscopy (SEM) visualization shows that the particles have self-assembled into monolayer islands in the middle of the droplet, as shown in Figure 1c. Each monolayer island consists of tens of particles. Blade-casting was performed using a custom precision instrument consisting of stationary glass blade and a motorized stage, as detailed in the Supporting Information. Hydrophilic silicon wafer substrates were mounted onto the motorized stage, and a glass microscope slide was suspended 0.005 in. above the substrate, at a 45° angle. A small amount (5 μL) of SiO_2AuNP solution was deposited at the gap between the blade and the substrate, and horizontal stage motion was initiated immediately, drawing the meniscus laterally across the substrate to induce convective self-assembly. Convective self-assembly by blade-casting can be optimized to form monolayers by matching the substrate speed to the natural rate of monolayer crystal growth v_c, which in turn depends on the rate of evaporation of water J_e, the particle diameter d, and the volume fraction of particles ϕ.[16−18] By considering the flux of water and particles transported to the edge of the meniscus by evaporation, Dimitrov and Nagayama proposed the following equation:

$$v_c = \frac{\beta J_e \phi}{0.605 d(1 - \phi)}$$

where β is a coefficient depending on particle−particle and particle−substrate interactions. β should approach unity for dilute suspensions such as in the particle solutions used in our experiments. We note that the optimal casting speed is dependent on a range of specific experimental conditions such as particle size, blade angle, temperature, and surface energy of the substrate.[16,19] While these experimental factors have been thoroughly investigated in other works, for our purposes, we vary casting speed while keeping the other factors constant. Under optimized conditions, we observe monolayer regions exceeding 1000 μm^2, as shown in Figure 1d.

Even though large monolayers can be made with blade-casting, it is very rare that the monolayer will cover the entire substrate because of the narrow range of conditions that must be met to sustain the natural assembly mode for monolayer continuity.[20] We observed that the monolayers tend to form as striations, as shown in Figure 2. In the SEM images, the lighter regions are monolayers, while the darker regions are multi-

DOI: 10.1021/acsanm.9b00184
ACS Appl. Nano Mater. 2019, 2, 1146−1151

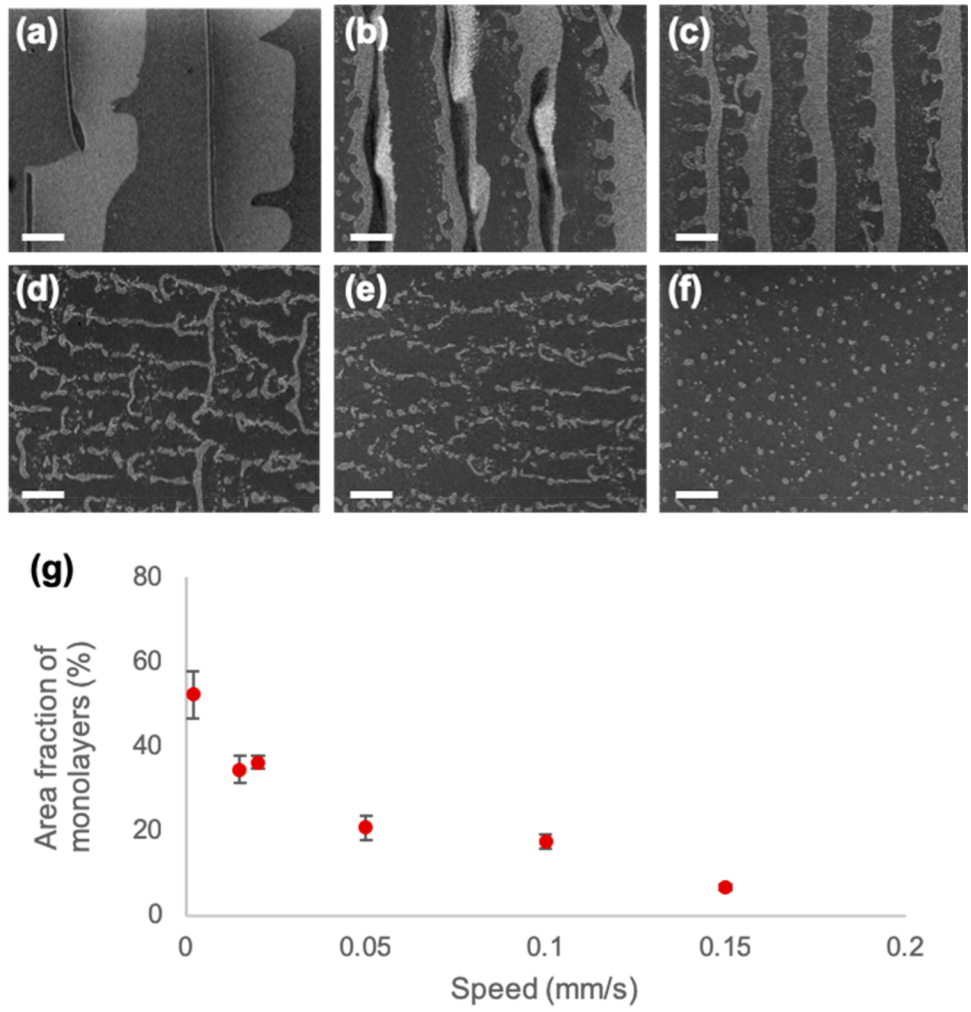

Figure 2. SEM images of blade-cast silicon produced using substrate speeds of (a) 0.002, (b) 0.015, (c) 0.02, (d) 0.05, (e) 0.1, and (f) 0.15 mm/s. Scale bars represent 10 μm. (g) Plot of area fraction of monolayer against casting speed, as obtained by the image analysis of SEM images. Error bars are standard deviations.

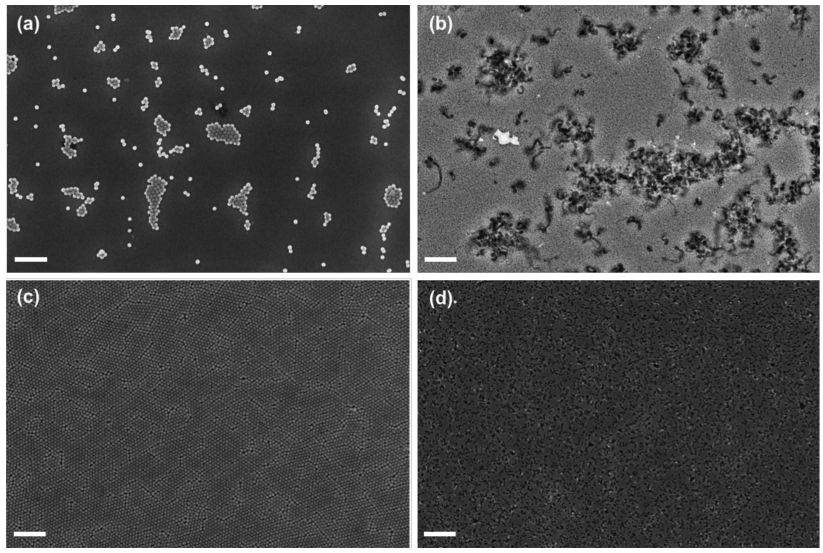

Figure 3. Effect of monolayer size on MACE-induced porosity. (a) SEM of 10 nm silica-shell gold-core nanoparticles (SiO_2AuNP) deposited on silicon substrates by drop-casting and (b) the corresponding SEM of the center of the drop-cast film after MACE. (c) SEM of SiO_2AuNP blade-casted over a silicon substrate and (d) the corresponding SEM of the surface of the substrate after MACE. Scale bars represent 500 nm.

DOI: 10.1021/acsanm.9b00184
ACS Appl. Nano Mater. 2019, 2, 1146−1151

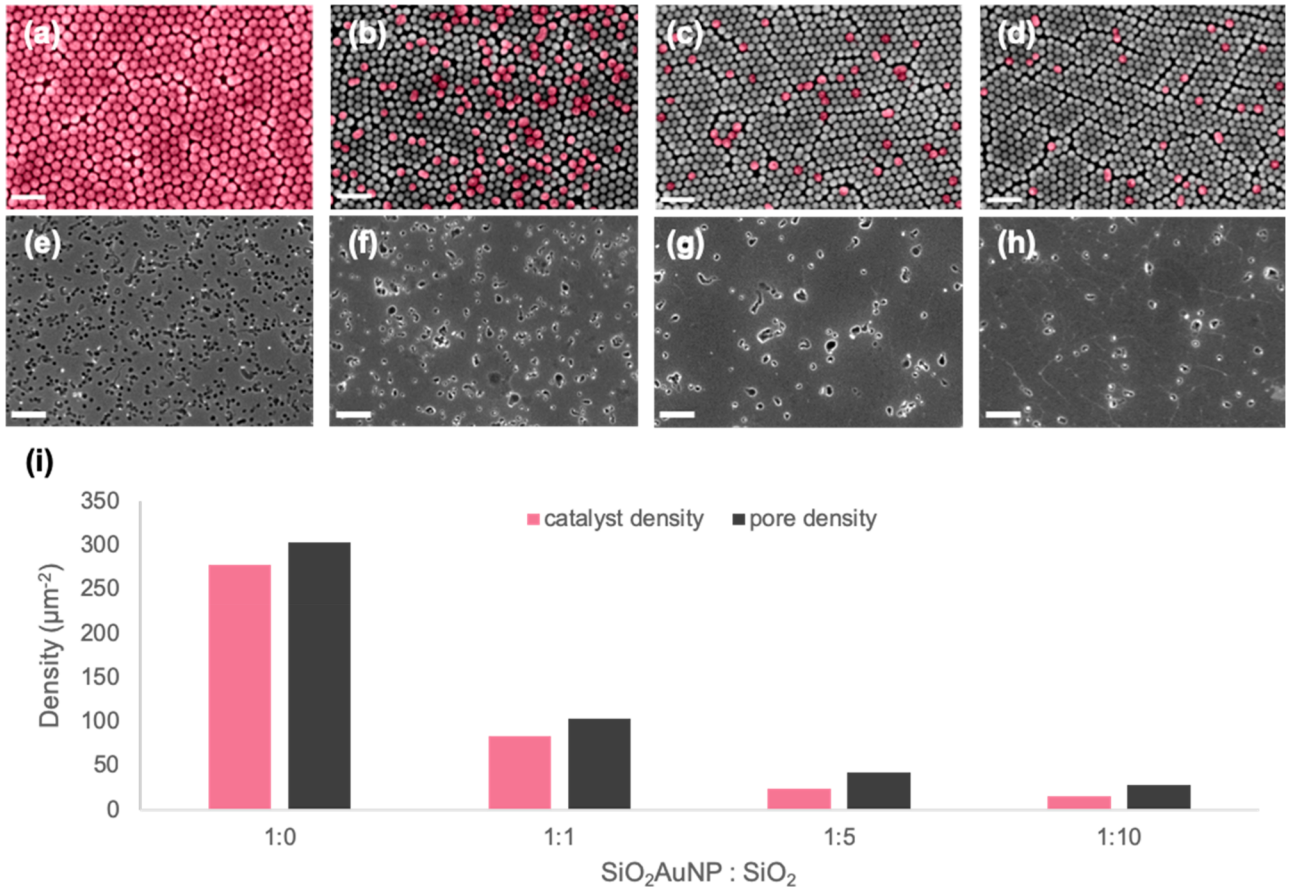

Figure 4. Tuning monolayer composition to tune porosity of NPSi. (a–d) SEM images of monolayers consisting of SiO_2AuNPs and SiO_2 particles in the ratios of 1:0, 1:1, 1:5, and 1:10, respectively. SiO_2AuNP particles are highlighted in red. (e–h) Corresponding SEMs of the silicon surface post-MACE. Scale bars represent 200 nm. (i) Number density of catalyst particles and pores as a function of ratio of SiO_2AuNPs to SiO_2 particles.

layers. Low speeds create striations of monolayers and multilayers that are parallel to the blade. Increasing the speed results in a gradual change to orient the pattern perpendicular to the blade. Low speeds result in dense multilayer and monolayer formation (Figure 2a–c), while higher speeds result in sparse monolayers (Figure 2d–f). The occurrence of striations during dewetting is well-documented in the literature[15,21−24] and is consistent with our results. At low speeds, the striations parallel to the blade form due to an oscillating slip-stick motion of the drying front.[21−24] At higher speeds, striations perpendicular to the drying front form due to a fingering instability.[15,25,26] One can anticipate that at intermediate speeds, there is a combination of slip-stick dewetting and fingering instability, as we do indeed observe in Figure 2c,d. At speeds above 0.1 mm/s, we observe isolated islands of particles, similar to that seen in the center of a drop-cast film.

We also note that, by varying casting speed, not only does the pattern of particle deposit qualitatively change, but also, the area coverage of particle monolayers changes. The effect of casting speed on monolayer area fraction is plotted in Figure 2g. As casting speed increases, the striations become thinner due to insufficient drying time. Therefore, the area coverage of monolayer decreases. Below 0.02 mm/s, the monolayer coverage increases but we also observe that thick multilayers also start to form, as shown in Figure 2a,b. For the purpose of forming monolayers without the occurrence of multilayers, which is important for the subsequent MACE process, we found a casting speed of 0.02 mm/s to be optimal.

To fabricate NPSi, MACE was performed by submerging the SiO_2AuNP-coated silicon substrates into a mixture of HF and H_2O_2. The effect of monolayer size on NPSi porosity is striking. Small and isolated monolayer islands deposited by drop-casting (Figure 3a) translate into disordered porous structures (Figure 3b). This is consistent with other works showing that isolated catalyst structures result in non-uniform hole injection into the underlying Si at the edges of the catalyst structure, leading to non-uniform etch rates and splaying of the resulting etch features.[27−29] In contrast, large close-packed monolayers deposited by blade-casting translate into an ordered porous structure due to uniform hole concentrations throughout the array of catalyst particles.

A pair of important pieces of information are gained from this experimental observation: First, large monolayers of the core–shell particles are necessary to constrain and "lock in" the gold catalyst particles for the etching of uniform pores normal to the surface. Second, tuning pore density is non-trivial. Deposition of isolated single particles from solution is difficult because the particles tend to self-assemble into islands, even when the particle solution is dilute. The islands of particles are not well-constrained and can still skid laterally during MACE, resulting in non-uniform, tortuous pores.

Therefore, there is a dilemma for tuning the porosity of NPSi using self-assembled SiO_2AuNP: the SiO_2AuNPs must be close-packed in a large monolayer to constrain the Au core

DOI: 10.1021/acsanm.9b00184
ACS Appl. Nano Mater. 2019, 2, 1146−1151

and prevent lateral motion of the particles during MACE. However, a close-packed arrangement of SiO_2AuNP particles limits the tunability of spacing between the Au cores, and the resulting density of pores after MACE. In essence, the pore density of nanoporous silicon cannot be controlled simply by depositing a more dilute suspension of metal particles because of the tendency of the metal particles to deposit in small clusters, resulting in merged pores after MACE.

We resolve this dilemma with a hierarchical approach to self-assembly where we blade-cast a mixture of SiO_2AuNP and SiO_2 particles. At the first level of hierarchy, the size and shape of monolayer coverage, i.e., pattern of the monolayer, can be tuned via controlled evaporative assembly by blade-casting, as we have elucidated above. At the second level of hierarchy, the space between the Au cores can be tuned by assembling a monolayer consisting of two particle types: SiO_2AuNP and SiO_2 particles. The SiO_2 particles act as inactive spacers between the SiO_2AuNPs.

We investigated the effect of tuning relative concentrations of SiO_2AuNP particles and SiO_2 particles by blade-casting with four different solutions: pure SiO_2AuNPs and mixtures of SiO_2AuNPs to SiO_2 in the ratios of 1:1, 1:5, and 1:10. To ensure a close-packed monolayer, the SiO_2AuNP particles and SiO_2 particles were chosen to be the same outer diameter. The resulting monolayers were imaged with SEM, as shown in Figure 4a–d. The gold cores are visible due to the penetration depth of the electron beam, thus allowing the SiO_2AuNP particles to be identified. For convenient visualization, in Figure 4, the SiO_2AuNP particles are highlighted in red. It is readily apparent that both the density of SiO_2AuNP particles in the monolayer and the pore density in the subsequently etched Si decreases with decreasing ratio of SiO_2AuNPs to SiO_2. Image analysis reveals monolayer catalyst densities of 277, 84, 24, and 16 μm^{-2} and corresponding pore densities of 304, 104, 42, and 29 μm^{-2} for the respective solutions (Figure 4i). It can therefore be concluded that a lower proportion of SiO_2AuNP particles relative to SiO_2 particles in the initial solution effectively decreases the proximity of neighboring SiO_2AuNP particles in the blade-cast monolayer. Such tunability is beneficial across many applications, in which either the prevention of etch-channel merging or broad control over pore density is desirable. Investigating the depth of the pores and the straightness of the etch channels would be an interesting topic of further study.

CONCLUSIONS

In conclusion, blade-casting can be implemented to create Au catalyst particle monolayers with tunable hierarchical structuring for the purpose of producing large area controllable porosity in NPSi via the MACE process. By controlling the assembly over two length scales, i.e., co-assembly of SiO_2AuNP and SiO_2 particles in the nanoscale, and the size of the monolayer on the micron scale, we have presented a facile, deterministic, and reproducible approach for fabricating nanoporous silicon with tunable porosity. Because the spacing between the SiO_2AuNP particles directly correlates with pore spacing in the NPSi after MACE, in future work, the distribution of SiO_2AuNP particles among SiO_2 particles can be potentially be controlled by functionalizing the particles with ligands capable of complementary interaction.[30] The ability to fabricate large areas of NPSi and tune its porosity will advance the development of NPSi for applications such as in nanofiltration. More broadly, hierarchical organization of catalyst particles such as gold cores can be useful in other processes with downstream fabrication steps. In this example, we demonstrated top-down fabrication of nanoporous silicon. Other applications, such as the spatially deterministic growth of nanotubes and nanowires, may be envisioned as well.

ASSOCIATED CONTENT

Supporting Information

The Supporting Information is available free of charge on the ACS Publications website at DOI: 10.1021/acsanm.9b00184.

Additional details on experimental methods and an optical image of drop-casted SiO_2AuNP (PDF)

AUTHOR INFORMATION

Corresponding Authors

*E-mail: ajhart@mit.edu.

*E-mail jcg@mit.edu.

ORCID

Alvin T.L. Tan: 0000-0002-8484-7107

Brendan D. Smith: 0000-0001-5255-6957

A. John Hart: 0000-0002-7372-3512

Author Contributions

§M.S. and A.T.L.T. contributed equally. The manuscript was written through contributions of all authors. All authors have given approval to the final version of the manuscript.

Notes

The authors declare no competing financial interest.

ACKNOWLEDGMENTS

M.S., B.D.S., and J.C.G. are grateful for the partial support from the Masdar Institute & MIT Cooperative Program. M.S. and B.D.S. also receive support from the MIT Tata Center for Technology and Design, as well as the Natural Sciences and Engineering Research Council of Canada. A.T.L.T. acknowledges a postgraduate fellowship from the Singapore Defence Science Organization. The authors thank Jamison Go and Dr. Mostafa Bedewy for design and fabrication of the blade-casting apparatus, which was supported by a National Science Foundation (NSF) CAREER award to A.J.H. (CMMI-1346638). The work was performed in part at the Center for Nanoscale Systems (CNS), a member of the National Nanotechnology Coordinated Infrastructure Network (NNCI), which is supported by the NSF under award no. 1541959. CNS is part of Harvard University.

ABBREVIATIONS

AuNP, gold nanoparticle;; NPSi, nanoporous silicon;; MACE, metal-assisted chemical etching;; SiO_2AuNP, silica shell gold core nanoparticle

REFERENCES

(1) Yuan, H. C.; Yost, V. E.; Page, M. R.; Stradins, P.; Meier, D. L.; Branz, H. M. Efficient Black Silicon Solar Cell with a Density-Graded Nanoporous Surface: Optical Properties, Performance Limitations, and Design Rules. *Appl. Phys. Lett.* **2009**, *95*, 123501.

(2) Otto, M.; Algasinger, M.; Branz, H.; Gesemann, B.; Gimpel, T.; Füchsel, K.; Käsebier, T.; Kontermann, S.; Koynov, S.; Li, X.; et al. Black Silicon Photovoltaics. *Adv. Opt. Mater.* **2015**, *3*, 147–164.

(3) Gaborski, T. R.; Snyder, J. L.; Striemer, C. C.; Fang, D. Z.; Hoffman, M.; Fauchet, P. M.; McGrath, J. L. High-Performance Separation of Nanoparticles with Ultrathin Porous Nanocrystalline Silicon Membranes. *ACS Nano* **2010**, *4*, 6973–6981.

DOI: 10.1021/acsanm.9b00184
ACS Appl. Nano Mater. 2019, 2, 1146–1151

(4) Achar, B. H. V.; Sengupta, S.; Bhattacharya, E. Fabrication of Ultrathin Silicon Nanoporous Membranes and Their Application in Filtering Industrially Important Biomolecules. *IEEE Trans. Nanotechnol.* **2013**, *12*, 583−588.
(5) Striemer, C. C.; Gaborski, T. R.; McGrath, J. L.; Fauchet, P. M. Charge- and Size-Based Separation of Macromolecules Using Ultrathin Silicon Membranes. *Nature* **2007**, *445*, 749−753.
(6) Lee, J.; Lim, J.; Yang, P. Ballistic Phonon Transport in Holey Silicon. *Nano Lett.* **2015**, *15*, 3273−3279.
(7) Lee, J. H.; Galli, G. A.; Grossman, J. C. Nanoporous Si as an Efficient Thermoelectric Material. *Nano Lett.* **2008**, *8*, 3750−3754.
(8) Smith, B. D.; Patil, J. J.; Ferralis, N.; Grossman, J. C. Catalyst Self-Assembly for Scalable Patterning of Sub 10 Nm Ultrahigh Aspect Ratio Nanopores in Silicon. *ACS Appl. Mater. Interfaces* **2016**, *8*, 8043−8049.
(9) Huang, Z.; Geyer, N.; Werner, P.; De Boor, J.; Gösele, U. Metal-Assisted Chemical Etching of Silicon: A Review. *Adv. Mater.* **2011**, *23*, 285−308.
(10) Deegan, R. D.; Bakajin, O.; Dupont, T. F.; Huber, G.; Nagel, S. R.; Witten, T. A. Capillary Flow as the Cause of Ring Stains from Dried Liquid Drops. *Nature* **1997**, *389*, 827−829.
(11) Bigioni, T. P.; Lin, X.-M.; Nguyen, T. T.; Corwin, E. I.; Witten, T. A.; Jaeger, H. M. Kinetically Driven Self Assembly of Highly Ordered Nanoparticle Monolayers. *Nat. Mater.* **2006**, *5*, 265−270.
(12) Jiang, P.; McFarland, M. J. Large-Scale Fabrication of Wafer-Size Colloidal Crystals, Macroporous Polymers and Nanocomposites by Spin-Coating. *J. Am. Chem. Soc.* **2004**, *126*, 13778−13786.
(13) Jiang, P.; Prasad, T.; McFarland, M. J.; Colvin, V. L. Two-Dimensional Nonclose-Packed Colloidal Crystals Formed by Spincoating. *Appl. Phys. Lett.* **2006**, *89*, 011908.
(14) Szekeres, M.; Kamalin, O.; Schoonheydt, R. A.; Wostyn, K.; Clays, K.; Persoons, A.; Dekany, I. Ordering and Optical Properties of Monolayers and Multilayers of Silica Spheres Deposited by the Langmuir-Blodgett Method. *J. Mater. Chem.* **2002**, *12*, 3268−3274.
(15) Huang, J.; Kim, F.; Tao, A. R.; Connor, S.; Yang, P. Spontaneous Formation of Nanoparticle Stripe Patterns through Dewetting. *Nat. Mater.* **2005**, *4*, 896−900.
(16) Prevo, B. G.; Velev, O. D. Controlled, Rapid Deposition of Structured Coatings from Micro- and Nanoparticle Suspensions. *Langmuir* **2004**, *20*, 2099−2107.
(17) Dimitrov, A. S.; Nagayama, K. Steady-State Unidirectional Convective Assembling of Fine Particles into Two-Dimensional Arrays. *Chem. Phys. Lett.* **1995**, *243*, 462−468.
(18) Dimitrov, A. S.; Nagayama, K. Continuous Convective Assembling of Fine Particles into Two-Dimensional Arrays on Solid Surfaces. *Langmuir* **1996**, *12*, 1303−1311.
(19) Bedewy, M.; Hu, J.; Hart, A. J. Precision Control of Nanoparticle Monolayer Assembly: Optimizing Rate and Crystal Quality. *2017 IEEE 17th International Conference on Nanotechnology, NANO 2017* **2017**, 286−289, DOI: 10.1109/NANO.2017.8117489.
(20) Brewer, D. D.; Shibuta, T.; Francis, L.; Kumar, S.; Tsapatsis, M. Coating Process Regimes in Particulate Film Production by Forced-Convection-Assisted Drag-Out. *Langmuir* **2011**, *27*, 11660−11670.
(21) Farcau, C.; Moreira, H.; Viallet, B.; Grisolia, J.; Ressier, L. Tunable Conductive Nanoparticle Wire Arrays Fabricated by Convective Self-Assembly on Nonpatterned Substrates. *ACS Nano* **2010**, *4*, 7275−7282.
(22) Ray, M. A.; Kim, H.; Jia, L. Dynamic Self-Assembly of Polymer Colloids to Form Linear Patterns. *Langmuir* **2005**, *21*, 4786−4789.
(23) Grisolia, J.; Viallet, B.; Amiens, C.; Baster, S.; Cordan, A. S.; Leroy, Y.; Soldano, C.; Brugger, J.; Ressier, L. 99% Random Telegraph Signal-like Noise in Gold Nanoparticle μ-Stripes. *Nanotechnology* **2009**, *20*, 355303.
(24) Lawrence, J.; Pham, J. T.; Lee, D. Y.; Liu, Y.; Crosby, A. J.; Emrick, T. Highly Conductive Ribbons Prepared by Stick−Slip Assembly of Organosoluble Gold Nanoparticles. *ACS Nano* **2014**, *8*, 1173−1179.
(25) Samid-Merzel, N.; Lipson, S. G.; Tannhauser, D. S. Pattern Formation in Drying Water Films. *Phys. Rev. E: Stat. Phys., Plasmas, Fluids, Relat. Interdiscip. Top.* **1998**, *57*, 2906−2913.
(26) Pauliac-Vaujour, E.; Stannard, A.; Martin, C. P.; Blunt, M. O.; Notingher, I.; Moriarty, P. J.; Vancea, I.; Thiele, U. Fingering Instabilities in Dewetting Nanofluids. *Phys. Rev. Lett.* **2008**, *100*, 176102.
(27) Lianto, P.; Yu, S.; Wu, J.; Thompson, C. V.; Choi, W. K. Vertical Etching with Isolated Catalysts in Metal-Assisted Chemical Etching of Silicon. *Nanoscale* **2012**, *4*, 7532.
(28) Huang, Z.; Geyer, N.; Werner, P.; de Boor, J.; Gösele, U. Metal-Assisted Chemical Etching of Silicon: A Review. *Adv. Mater.* **2011**, *23*, 285−308.
(29) Chang, C.; Sakdinawat, A. Ultra-High Aspect Ratio High-Resolution Nanofabrication for Hard X-Ray Diffractive Optics. *Nat. Commun.* **2014**, *5*, 4243.
(30) Zhang, J.; Santos, P. J.; Gabrys, P. A.; Lee, S.; Liu, C.; Macfarlane, R. J. Self-Assembling Nanocomposite Tectons. *J. Am. Chem. Soc.* **2016**, *138*, 16228.

DOI: 10.1021/acsanm.9b00184
ACS Appl. Nano Mater. 2019, 2, 1146−1151